

# We are IntechOpen, the world's leading publisher of Open Access books Built by scientists, for scientists

6,900

Open access books available

186,000

International authors and editors

200M

Downloads

Our authors are among the

154

Countries delivered to

TOP 1%

most cited scientists

12.2%

Contributors from top 500 universities



WEB OF SCIENCE™

Selection of our books indexed in the Book Citation Index  
in Web of Science™ Core Collection (BKCI)

Interested in publishing with us?  
Contact [book.department@intechopen.com](mailto:book.department@intechopen.com)

Numbers displayed above are based on latest data collected.  
For more information visit [www.intechopen.com](http://www.intechopen.com)



---

# Copper Indium Gallium Selenide Thin Film Solar Cells

---

Yang Tang

Additional information is available at the end of the chapter

<http://dx.doi.org/10.5772/65291>

---

## Abstract

The solar energy as one of the new energy sources and a regenerated energy is abundant and pollution-free. Most photovoltaic devices (solar cells) sold in the market today are based on silicon wafers, the so-called "first generation" technology. The market at present is on the verge of switching to a "second generation" of thin film solar cell technology which offers prospects for a large reduction in material costs by eliminating the costs of the silicon wafers. Cadmium telluride (CdTe), amorphous silicon (a-Si) and copper indium gallium selenide (CIGS) are three thin film technologies which have achieved commercial production. This chapter gives the review of the CIGS solar cells regarding the heterostructures, materials, technology and research advances. It also states the key findings in our research and provides suggestions for future research.

**Keywords:** Cu(In,Ga)(S,Se)<sub>2</sub>, solar cell, thin film, photon management, carrier collection, nanostructure

---

## 1. Introduction

Nowadays the development of the society and economy raises up the dependence upon the energy sources. However, the energy crisis and the environmental problems induced by using the fossil energy sources have attracted much attention. A consensus about developing new energy as well as the reduction of the fossil energy consumption has been reached all over the world. The solar energy as one of the new energy sources and a regenerated energy is abundant and pollution-free. Photovoltaics (PV) is a method of generating electrical power through transforming solar energy into direct current electricity. The transformation is achieved by using semiconductors that exhibit the photovoltaic effect. The photovoltaic effect refers to photons of light exciting electrons into a higher state of energy, allowing them to act as charge carriers for an electric current. Most photovoltaic devices (solar cells) sold in the market today are based on

---

silicon wafers. There is an argument that the silicon solar cells are the so-called “first generation” technology. The market at present is on the verge of switching to a “second generation” of thin film solar cell technology which offers prospects for a large reduction in material costs by eliminating the costs of the silicon wafers. However, whether the thin film solar cell can be attributed to a “second generation” technology is still a controversial issue. Despite the debate, the silicon photovoltaic industry has reached its industrial maturity. The approach to progress further is to increase the efficiency as well as decrease the cost of the solar cells. The thin film photovoltaic technology is one of the potential alternative approaches.

Classification	Area (cm <sup>2</sup> ) <sup>a</sup>	Efficiency (%)	References
Cu(In,Ga)Se <sub>2</sub> (cell)	0.5 (unknown)	22.3	[2]
Cu(In,Ga)Se <sub>2</sub> (module)	808 (da)	17.5	[3]
CdTe (cell)	Unknown	22.1	[4]
CdTe (module)	Unknown	18.6	[5]
a-Si (cell) <sup>b</sup>	1.043 (da)	13.6	[6]
a-Si (module) <sup>c</sup>	14322 (t)	12.3	[7]
Dye sensitized (cell)	1.005 (da)	11.9	[8]
Dye sensitized (minimodule)	26.55 (da)	10.7	[8]
Organic (cell)	0.0429 (ap)	11.5	[9]
Organic (module)	802 (da)	8.7	[10]
Perovskite (cell)	Unknown	22.0	[11]

<sup>a</sup> ap = aperture area; da = designated illumination area (defined in [1]); t = total area.

<sup>b</sup> a-Si/nc-Si/nc-Si triple junction solar cell.

<sup>c</sup> a-Si/nc-Si tandem solar cell.

**Table 1.** The efficiency table of the thin-film solar cells.

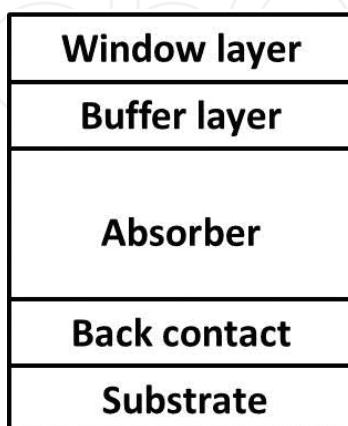


**Figure 1.** The cell structure of the Cu(In,Ga)Se<sub>2</sub> solar cell.

Currently three types of the thin film solar cells have realized industrialization. They are cadmium telluride (CdTe) solar cells, amorphous silicon (a-Si) solar cells and copper indium gallium diselenide (CIGS) solar cells. The other thin film technologies such as perovskite solar cells, dye-sensitized solar cells (DSSCs), organic solar cells and quantum-dot solar cells (QDSCs) remain in the stage of lab research or pilot line. The a-Si solar cells in the PV industry are fading away because of its relative low efficiency and instability. The CdTe and CIGS solar cells show the rapid development trend in recent years. **Table 1** presents the efficiencies of different thin film solar cells. Among them, the CIGS solar cells show the highest efficiency both in cells and modules.

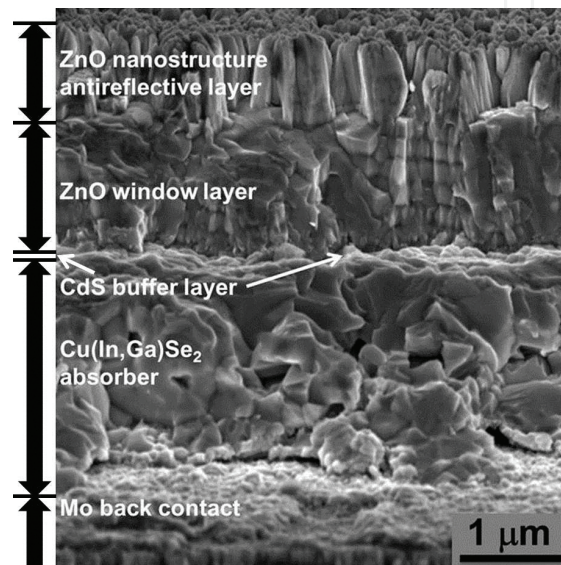


**Figure 2.** The image of the layers in the CIGS solar cell by scanning electron microscopy.

The structure of the CIGS solar cells is shown in **Figure 1**. The CIGS solar cells consist of a number of films which are deposited onto a rigid or flexible substrate. The first film, typically molybdenum (Mo), serves as a nontransparent back-contact. It is covered by the actual  $\text{Cu(In,Ga)Se}_2$  film. Most of the light is absorbed by the p-type thin film (absorber) and the photocurrent is generated. The heterojunction is formed by depositing a very thin n-type buffer layer (typically CdS) and an n-type wide gap transparent window layer (usually heavily doped ZnO). **Figure 2** presents the actual image of the layers in the CIGS solar cell, which is measured by a scanning electron microscopy (SEM). From the bottom to the top, they are Mo back contact layer,  $\text{Cu(In,Ga)Se}_2$  absorber layer, a very thin CdS buffer layer, the ZnO window layer and ZnO nanostructure antireflective coating layer.

## 2. Fundamental properties of the key materials

The definition of the thin-film given by Chopra et al. [12] provides a good starting point and also yields a criterion to discriminate the term ‘thin film’ from ‘thick film’. According to their

opinion, a thin film is defined as a material that is created ab initio by the random nucleation and growth processes of individually condensing/reacting atomic/ionic/molecular species on a substrate. Thin films may encompass a considerable thickness range, varying from a few nanometers to tens of micrometers and thus are best defined in terms of the production processes rather than by thickness. The layers for constructing the CIGS solar cells are back contact layer, absorber layer, buffer layer and window layer.

### 2.1. Back contact layer

The back contact layer as the back contact electrode of the solar cell is usually deposited on the substrate such as glass or flexible foils. One of the key requirements for the back contact layer is that the contact between the back contact and the absorber layer should be ohmic contact. The back contact layer should have a good conductivity and can be adhered to substrate firmly in order to make the solar cell stable. Molybdenum (Mo) is used in the majority of the CIGS solar cells. The structural and morphological properties of the Mo thin films will greatly affect the sequent growth of the absorber layer.

### 2.2. Absorber layer

The absorber layer is deposited on the back contact layer.  $\text{CuInSe}_2$  (CIS) was the first absorber layer developed in the 1970s. In the next two decades gallium was introduced into the absorber layer, resulting in the deposition of the  $\text{Cu(In,Ga)Se}_2$  thin films. The invention of the new generation absorber layer boosted the solar cells' efficiency by increasing the absorber's band gap. In addition, the possibility of fabricating graded band gap  $\text{Cu(In,Ga)Se}_2$  absorber layer further increased the device efficiency. Several other improvements were developed such as the thinner CdS buffer layer (less than 50 nm) and the use of the soda lime glass during this period. These technologies resulted in the progress of the  $\text{Cu(In,Ga)Se}_2$  absorber layer's performance.

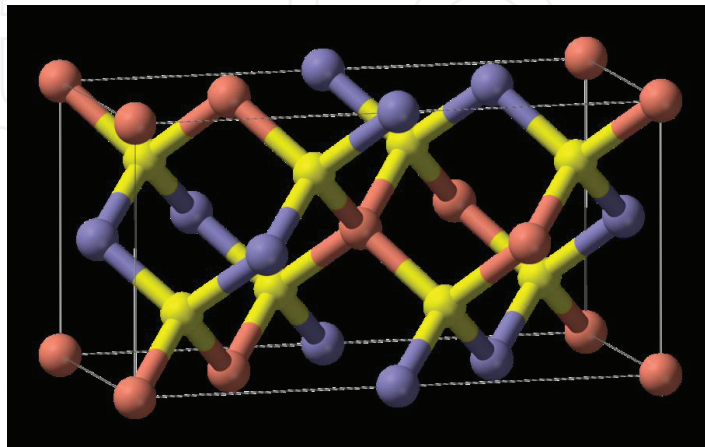


**Figure 3.** The  $\text{Cu(In,Ga)Se}_2$  crystal structure. Red = Cu, yellow = Se, blue = In/Ga [13].

The Cu(In,Ga)Se<sub>2</sub> material possesses a chalcopyrite crystal structure which is shown in **Figure 3**. Each anion (Se) is coordinated by two cations of each type (Cu, In/Ga). The Cu(In,Ga)Se<sub>2</sub> is obtained by partially replacing indium in a CIS structure with Ga. Since the atomic radii of the Ga are smaller than In, the lattice constants will be decreased with increasing Ga content.

The band gap of the Cu(In,Ga)Se<sub>2</sub> material depends on the ratio of Cu/(In + Ga). The band gaps of CuInSe<sub>2</sub> and CuGaSe<sub>2</sub> are 1.02 and 1.67 eV, respectively. The band gap of the Cu(In,Ga)Se<sub>2</sub> varies between 1.02 and 1.67 eV by the change in Ga/(In + Ga) ratio.

### 2.3. Buffer layer

The buffer layer is deposited on the absorber layer. CdS is the most widely used buffer layer in the CIGS solar cells. CdS is an n-type semiconductor with a band gap of ~2.4 eV. The buffer layer improves the CIGS solar cells' performance by forming the optimized band alignment between the absorber layer and the window layer. In addition, the buffer layer possesses more advantages to the CIGS solar cells such as the damage prevention of the absorber layer in the sequent sputtering process, the passivation of the absorber surface, the relief of the lattice misfit and so on. Besides CdS, more new buffer layers are in the development process. For example, the new buffer layers include Zn(S,O), ZnMgO, ZnS and In<sub>2</sub>S<sub>3</sub>. Since the research on the new buffer layers is a hotspot in the development of the CIGS solar cell in recent years, one can search a lot of published papers regarding the new generation Cd-free buffer layers and some of them showed great progress.

### 2.4. Window layer

As the window layer, ZnO is deposited on the buffer layer in the CIGS solar cells. ZnO is not really a newly discovered material. Research on ZnO has continued for many decades with interest. In terms of its characterization, reports go back to 1935 or even earlier. For example, lattice parameters of ZnO were investigated for many decades [14–18].

Most of the group II–VI binary compound semiconductors crystallize in either cubic zinc blende or hexagonal wurtzite structure where each anion is surrounded by four cations at the corners of a tetrahedron, and vice versa. **Figure 4** depicts three kinds of crystal structures shared by ZnO which are rocksalt, zinc blende and wurtzite [19]. The zinc-blende ZnO structure can be stabilized only by growth on cubic substrates, and the rocksalt structure may be obtained at relatively high pressures [18].

The wurtzite structure has a hexagonal unit cell with two lattice parameters,  $a$  and  $c$ , in the ratio of  $c/a = \sqrt{8/3} = 1.633$  and belongs to the space group of  $C_{6v}^4$  or P6<sub>3</sub>mc. In a real ZnO crystal, the lattice parameters deviate from the ideal value due to the existence of the Zn interstitials, O vacancies and dislocations in the crystal structure. The properties vary with different material types (bulk material, thin films, powders and nanostructures) and different synthesis processes.

The window layers in the CIGS solar cells usually are consisted of two layers. The first layer deposited on the buffer layer is the intrinsic ZnO thin films. In the following an aluminum-doped ZnO (AZO) layer is deposited on the undoped ZnO layer. The AZO layer processing high conductivity will be used as the front contact for a CIGS module.

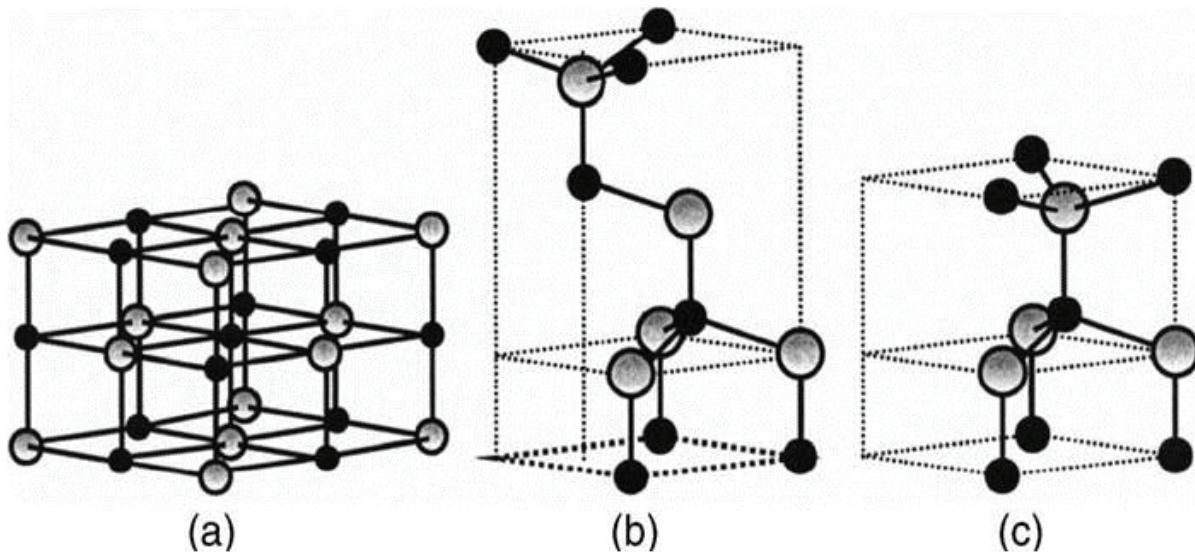


**Figure 4.** Stick and ball representation of ZnO crystal structures: (a) cubic rocksalt, (b) cubic zinc blende, (c) hexagonal wurtzite. The shaded gray and black spheres denote Zn and O atoms, respectively [19]. Copyright 2005 by AIP Publishing LLC.

### 3. Technology of the CIGS solar cells

The term "photo-voltaic" has been in use in English since 1849. A photovoltaic cell (also called a solar cell) is an electrical device that converts the energy of light directly into electricity by the photovoltaic effect [20]. The operation of a solar cell requires three basic attributes. At first, the absorption of light generates either electron-hole pairs or excitons. Afterwards, various types of charge carriers are separated. Finally, those carriers are extracted to an external circuit. Conventionally, photovoltaic materials use inorganic semiconductors. Ideally, the absorber material of an efficient solar cell should be a semiconductor with a bandgap of 1–1.5 eV with a high solar optical absorption ( $10^4$  to  $10^5$   $\text{cm}^{-1}$ ) in the wavelength region of 350–1000 nm, a high quantum yield for the excited carriers, a long diffusion length and low recombination velocity [21].

The magnetron sputtering is extensively used to deposit the Mo back contact layer and the ZnO window layer. The CdS buffer layer is usually fabricated by a chemical bath deposition method. Several more methods such as atomic layer deposition and spray ion layer gas reaction technique have been adopted to obtain the new buffer layers. Several techniques were developed to fabricate  $\text{Cu}(\text{In,Ga})\text{Se}_2$ . Among them the coevaporation method and the two-stage process are two of the most important techniques.

### 3.1. Coevaporation process

The brief setup of the coevaporation process is shown in **Figure 5**. During the process, Cu, In, Ga and Se sources are heated and evaporated to be grown on a heated substrate. The heating temperature is specific for each source. The temperature for Cu, In and Ga is higher than that for Se. It is very important to control the element flux in the coevaporation process. The in-situ feedback controls based on electron impact emission spectrometry, quadruple mass analysis or atomic absorption spectrometry have been successfully adopted to control the element flux. Although the progress for the coevaporation process is in rapid development, the problems regarding the process control in the absorber deposition remain to be improved.

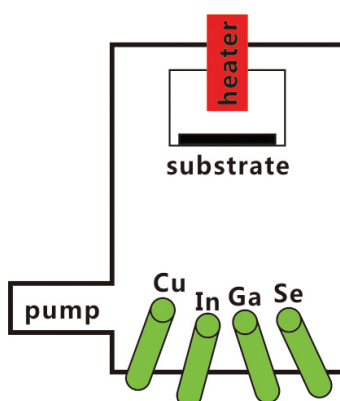


**Figure 5.** The setup of the coevaporation process.

### 3.2. Two-stage process

The two-stage process was invented by Boeing company. For the first stage, a stack of precursor layers including the Cu, In and Ga metals is deposited. In the following stage, the deposited precursor alloy layers are transferred to a furnace or a specific reaction setup for selenization. Either  $H_2Se$  gas or Se powders are used for selenization process. **Figure 6** shows the brief setup of the selenization furnace.

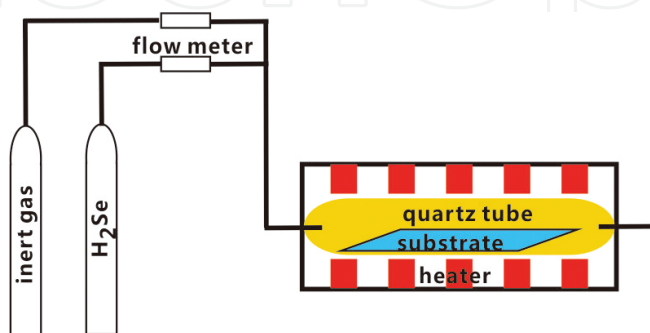


**Figure 6.** The setup of the selenization furnace.

## 4. Recent research advances

The approach to progress further is to increase the efficiency as well as decrease the cost of the solar cells. Therefore new concepts and new cell structures should be brought in the development of the film solar cells. One of the plausible solutions is to implant nanostructures in the conventional thin film photovoltaic devices. Zinc oxide (ZnO) nanorod arrays are one of the nanostructures that can be implanted in the solar cells. ZnO nanostructures can be grown on top of the CIGS solar cells' window layers as an antireflective coating layer or implanted into the solar cells. On the one hand, the implanted nanostructures will decrease the reflection and increase the light path due to light coupling effects. On the other hand, the ZnO nanostructures will put the electrode close to the photoinduced carrier generation area with larger carrier collection function. It will assist in boosting the solar cells' efficiency by carrier collection enhancement.

### 4.1. Photon management

Thin film photovoltaic device technology relies on light management to enhance light absorption in thin absorber layers. One of the plausible solutions is to implant nanostructures in the conventional thin film photovoltaic devices. For example, the zinc oxide (ZnO) nanorod arrays can be implanted in the CIGS solar cells. The use of the ZnO nanorods in the thin film solar cells is an effective way to decrease the reflection. The variation of the geometrical parameters of the ZnO nanorods, such as the diameter, the height and the density can lead to an optimum which results in the maximal absorption in the absorber. An approach of a rigorous three-dimensional (3D) modeling based on the finite element method (FEM) can be used to simulate and optimize the light absorption in the Cu(In,Ga)Se<sub>2</sub> absorbers with nanostructures.

Modeling the optical properties of the Cu(In,Ga)Se<sub>2</sub> absorbers with nanostructures starts by defining the characteristics of the incident light. In the stationary case, the electric and magnetic field can be expressed as follows.

$$\mathbf{E}(x, y, z, t) = \tilde{\mathbf{E}}(x, y, z)e^{-i\omega t} \quad (1)$$

$$\mathbf{H}(x, y, z, t) = \tilde{\mathbf{H}}(x, y, z)e^{-i\omega t} \quad (2)$$

where  $\mathbf{E}$  is the electric field,  $\mathbf{H}$  is the magnetic field and  $\omega$  is the angular frequency related by  $\omega = 2\pi f$  to the frequency  $f$  of light. The mathematical model of the light propagation is Maxwell's equation:

$$\mathbf{E}(x, y, z, t) = \tilde{\mathbf{E}}(x, y, z)e^{-i\omega t} \quad (3)$$

$$\nabla \cdot \mathbf{H} = 0 \quad (4)$$

$$\nabla \times \mathbf{E} = -\frac{\partial \mu \mathbf{H}}{\partial t} \quad (5)$$

$$\nabla \times \mathbf{H} = \mathbf{J} + \frac{\partial \epsilon \mathbf{E}}{\partial t} \quad (6)$$

where  $\mathbf{E}$  is the electric field,  $\mathbf{H}$  is the magnetic field,  $\rho$  is the electric charge density,  $\epsilon$  is the permittivity,  $\mu$  is the magnetic permeability and  $\mathbf{J}$  is the current density. In the time harmonic case the magnetic field can be determined by the electric field and vice versa. From Maxwell's equations we can find

$$\mathbf{H} = -\frac{1}{i\omega \epsilon} \nabla \times \mathbf{E} \quad (7)$$

$$\mathbf{E} = \frac{1}{i\omega \epsilon} \nabla \times \mathbf{H} \quad (8)$$

Thus the electric field in the electromagnetic will be taken into account in the simulation. The electric field distribution of the incident light is described by unpolarized stationary plane waves.

$$\tilde{\mathbf{E}} = A e^{i(\mathbf{k} \cdot \mathbf{r} + \phi)} \quad (9)$$

where  $A$  is the constant,  $\mathbf{k}$  is the wave vector,  $\mathbf{r}$  is the position vector and  $\phi$  is the phase angle. For simplifying the simulation, the wave vector of the incident light is perpendicular to the surface of the Cu(In,Ga)Se<sub>2</sub> absorbers and  $\phi$  is taken as 0.

The nanorod arrays as a light coupling component can be incorporated into two types of solar cells, i.e., the bifacial solar cells and the superstrate solar cells. As shown in **Figure 7(a)**, both sides of the bifacial solar cells are illuminated and the ZnO nanorods work as a light-coupling component and a nanocontact electrode. The intrinsic ZnO nanorods in the superstrate solar cells play a buffer role. Optionally a buffer layer can be inserted between the ZnO nanorods and the absorber in the superstrate solar cells. Since both the bifacial and superstrate solar cells possess the same components which are glass/transparent conductive oxides/ZnO nanorods/Cu(In,Ga)Se<sub>2</sub> absorber, the same components are regarded as the simulated structure. As illustrated in **Figure 7(c)**, the simulated structure can be divided into two parts: the glass and the transparent conductive oxides/ZnO nanorods/Cu(In,Ga)Se<sub>2</sub> absorber (TNA) structure.

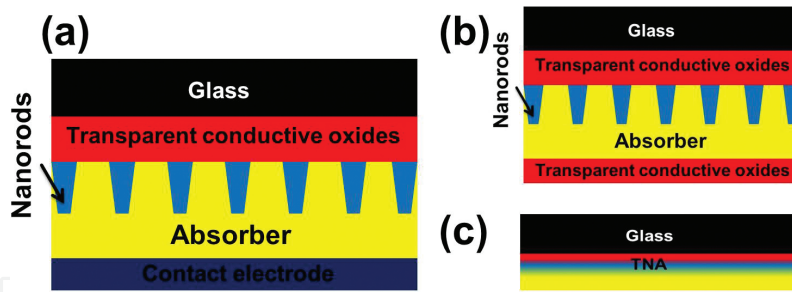


**Figure 7.** (a) The schematic structure of the bifacial Cu(In,Ga)Se<sub>2</sub> solar cell. (b) The schematic structure of the superstrate Cu(In,Ga)Se<sub>2</sub> solar cell. (c) The schematic drawing of the simulated structure. The TNA is the abbreviation for the transparent conductive oxides/nanorods/absorber.

As shown in **Figure 8**, the total reflection consists of the specular reflectance and the scattered reflectance:

$$R^{Total} = R^S + R^{SC} \tag{10}$$

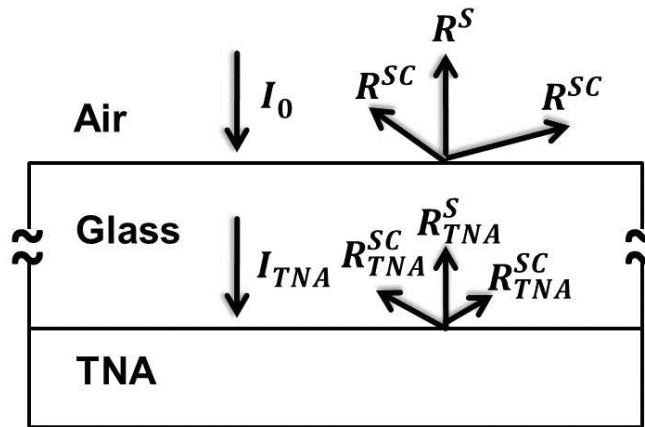


**Figure 8.** The schematic structure of the simulated structure. The structure is illuminated through the glass side. The figure defines the incident light intensity  $I_0$ , the specular intensity  $I_{TNA}$  illuminating the glass/TNA interface, the specular reflectance  $R^S$  the scattered reflectance,  $R^{SC}$  the specular reflectance of the  $R_{TNA}^S$  structure and the scattered reflectance of the  $R_{TNA}^{SC}$  structure.

where  $R^S$  and  $R^{SC}$  are the specular reflectance and the scattered reflectance, respectively. The specular reflectance is given as:

$$R^S = R_{glass} + (1 - R_{glass})^2 \cdot \tau_{glass}^2 \cdot R_{TNA}^S \cdot \sum_{u=0}^{\infty} [R_{glass} \cdot \tau_{glass}^2 \cdot R_{TNA}^S]^u \tag{11}$$

where  $R_{glass}$  is the reflectance at the air/glass interface with the incident of light illuminating the interface,  $\tau_{glass}$  is the absorptance of the thick glass and  $R_{TNA}^S$  is the reflectance of the TNA structure illuminated from the glass. The  $R_{glass}$  is calculated from the Fresnel's equation:

$$R_{glass} = \left| \frac{n_{glass} - 1}{n_{glass} + 1} \right|^2 \quad (12)$$

$$n_{glass} = n + i \cdot k \quad (13)$$

where  $n_{glass}$  is the complex refractive index of the glass,  $n$  is the refractive index of the glass and  $k$  is extinction coefficient of the glass. The  $\tau_{glass}$  is calculated as:

$$\tau_{glass} = \exp(-\alpha_{glass} \cdot d_{glass}) \quad (14)$$

$$\alpha_{glass} = \frac{4\pi k}{\lambda_0} \quad (15)$$

where  $\alpha_{glass}$  is the optical absorption coefficient of the glass and  $\lambda_0$  is the vacuum wavelength of light.

The reflection, transmission and absorption in TNA structure can be calculated using the finite element method (FEM) method. The FEM is a numerical technique used in finding solutions of Maxwell equations. The volume of the simulated structure is meshed and electromagnetic field components are computed. Once the simulation of the design (structure, boundary conditions, light sources and frequency range) is set up, FEM process operates through three steps: meshing, solving and postprocessing. In the first step, for a given wavelength, the volume of the designed structure is discretized. During the second step, the resulting system of the equations is solved. In the third step, the reflection, transmission and absorption of the simulated structure is computed. The reflectance  $R_{TNA}$  is given by:

$$R_{TNA} = R_{TNA}^S + R_{TNA}^{SC} \quad (16)$$

where  $R_{TNA}^{SC}$  is the scattered reflectance of the TNA structure. Since tracing the scattered reflected light of the TNA structure in the thick glass and air/glass interface dramatically boosts the computation amount, it is not possible to get the results using FEM. The total reflectance is approximately calculated as:

$$R^{Total} = R_{glass} + R_{TNA} \quad (17)$$

## 4.2. Nanostructures

An antireflective or antireflection coating (ARC) is a type of optical coating applied to the surface of lenses and other optical devices to reduce reflection. This improves the efficiency of the system since less light is lost. The ARC is generally made of a dielectric layer, e.g.,  $MgF_2$ ,  $SiN$ ,  $TiO_2$  or  $ZnS$ , with a thickness of a quarter-wavelength [22–25]. Another approach of

boosting light coupling is to structure the surface of the solar cells by means of the moth-eye effect. Moths' eyes have an unusual property: their surfaces are covered with a natural nanostructured film which eliminates reflections. The ZnO nanorods have an appropriate refractive index of  $\sim 2$ . Coating an absorber surface leads to continuously varying refractive index profiles in the tapered ZnO nanorods. Consequently they suppress the surface reflection via a subwavelength structure. Therefore the tapered ZnO nanorods are a promising light coupling layer for ARC of solar cells as well as solar thermal selective surfaces.

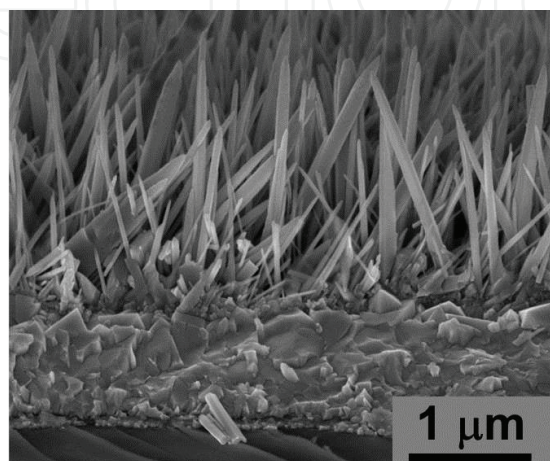


**Figure 9.** The ZnO nanowire arrays prepared by the hydrothermal method.

**Figure 2** has shown the cross section scanning electron microscopy (SEM) images of ZnO nanorods on CIGS. The ZnO nanorod arrays serving as an ARC were electrodeposited on thin film Cu(In,Ga)Se<sub>2</sub> solar cells. According to the research, the weighted reflectance was reduced from 8.6 to 3.5%. Highest increases in both the saturation-current of 5.7% and the solar cells efficiency of 7.2% were achieved [26]. In addition, the ZnO nanorod arrays have been incorporated into a superstrate or a bifacial cell structure of the other thin film photovoltaic devices such as DSSCs [27], QDSCs [28] and organic solar cells [29].

ZnO nanostructures have been prepared by various methods [30–46]. The solution-based fabrication routes including hydrothermal method and electrochemical deposition (ECD) method are the only ways to grow ZnO nanostructures at a low temperature down to the range between 60°C and 90°C [35–46]. Meanwhile the growth can be achieved over large areas up to 10 cm × 10 cm [44–46]. **Figure 9** shows the SEM image of the ZnO nanowire arrays prepared by the hydrothermal method.

The ECD technique consists of an electrochemical cell and accessories for providing a galvanic current which flows through the electrochemical cell. The cell usually contains electrolyte and electrodes. The first of these electrodes has been named the anode. At an anode, electrons go away from the electrolyte to the anode. Hence, an anodic reaction must generate electrons. The second has been named the cathode. The cathode supplies electrons to the positively charged cations which flow to it from the electrolyte. Within the electrolyte, the current flow is always from the anode to the cathode, which means the electron transports from the cathode to the

anode. In the external parts of the closed circuit (“external” relative to the electrolyte), the current flow is from cathode to anode, which equates the electron transport from the anode to the cathode [47].

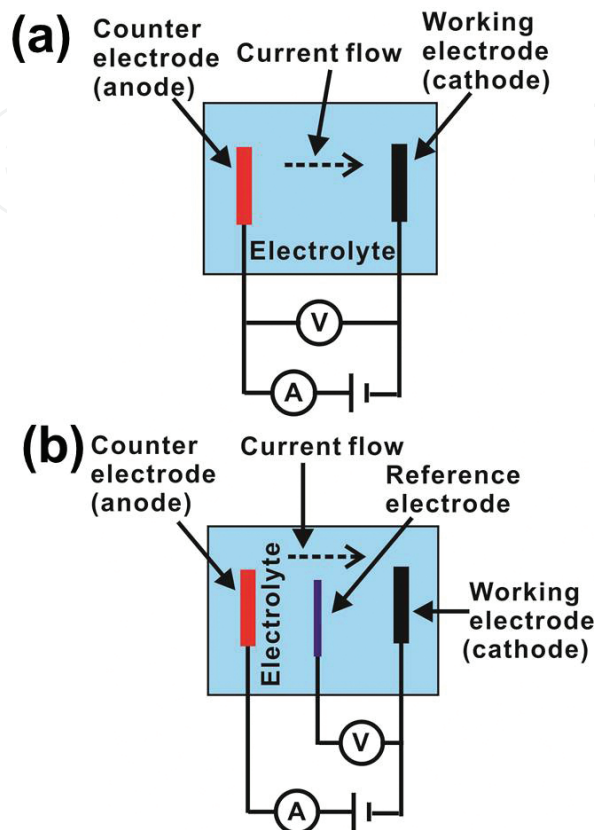


**Figure 10.** (a) Two-electrode system and (b) three-electrode system.

During the ECD process, the electrodeposited products are deposited on one of the electrodes. The electrode is the working electrode (WE). However, the WE is not enough for the ECD process. At least another electrode is necessary for allowing current to flow. In the simplest case a two-electrode cell is used for ECD (**Figure 10(a)**). The second electrode is used both as the reference electrode (RE) to measure the WE potential and as a counter electrode (CE) to allow current to flow. However, the potential of the second electrode changes accordingly when there is a current flow, which has been termed electrode polarization. In order to measure the accurate WE potential, a three-electrode cell containing a WE, a CE and a RE is more common (**Figure 10(b)**). A current flows between the WE and CE, while the potential of the WE is measured against the RE. No current flows in the circuit of the RE/WE, which therefore is not polarized [48]. The glass substrates coated by FTO and AZO transparent conductive oxides are used as the WE. The electrochemical cell was placed in a thermoregulated bath. The liquid electrolyte contains zinc salts and additives. During the experiments the liquid electrolyte in which there is a magnetic stirring bar is agitated. A schematic illustration of the setup for the ECD process is shown in **Figure 11**. The electrochemical process is controlled and recorded by a potentiostat/galvanostat.

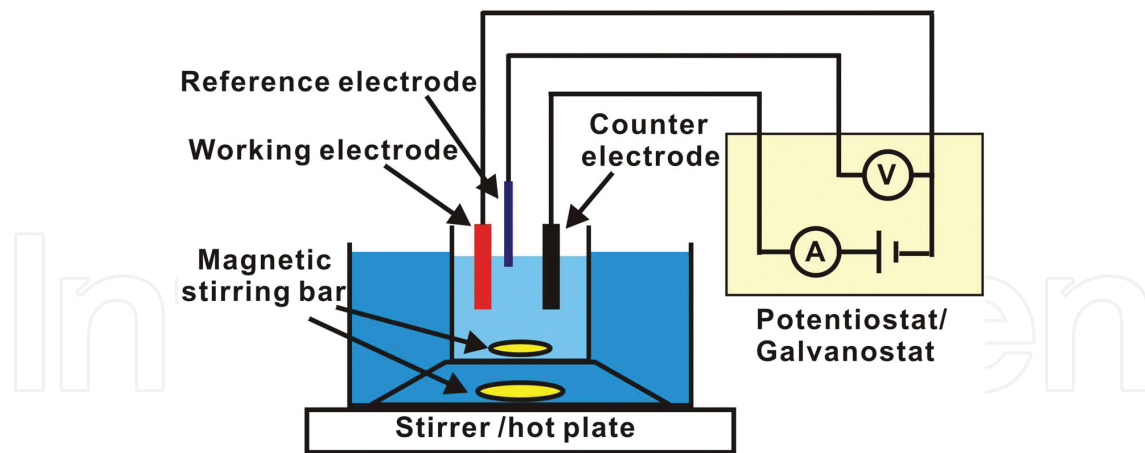


Figure 11. Schematic description of the electrochemical deposition setup.

## 5. Conclusion

This chapter gives the review of the CIGS solar cells regarding the heterostructures, materials, technology and research advances. The CIGS solar cells consist of a number of films which are deposited onto a rigid or flexible substrate. Mo deposited by magnetron sputtering serves as a nontransparent back-contact. The Mo film is covered by the actual  $\text{Cu}(\text{In,Ga})\text{Se}_2$  film. The coevaporation method and the two-stage process are two of the most important techniques to fabricate  $\text{Cu}(\text{In,Ga})\text{Se}_2$ . The heterojunction is formed by depositing a very thin n-type buffer layer (typically CdS) and an n-type wide gap transparent window layer (usually heavily doped ZnO). The CdS buffer layer is usually fabricated by a chemical bath deposition method. The magnetron sputtering is extensively used to deposit the ZnO window layer. The chapter also states the key findings in our research and provides suggestions for future research. One of the plausible solutions for boosting solar cells' efficiency is to implant nanostructures such as ZnO nanorod arrays in the conventional thin film photovoltaic devices. ZnO nanostructures can be grown on top of the CIGS solar cells' window layers as an antireflective coating layer or implanted into the solar cells. On one hand, the implanted nanostructures will decrease the reflection and increase the light path due to light coupling effects. On the other hand, the ZnO nanostructures will put the electrode close to the photoinduced carrier generation area with larger carrier collection function. It will assist in boosting the solar cells' efficiency by carrier collection enhancement.

## 6. Outlook

In the past four decades, the CIGS thin film solar cells have developed steadily. The lab efficiency of the CIGS solar cells has reached to as high as 22.6% [2]. However, the journey to successful large-scale commercialization is going through fire and water. Nowadays the silicon

photovoltaic industry has entered its maturity stage from the industry life cycle point of view. It is ambiguous to estimate that whether the CIGS thin film solar cell is in its introduction stage or in a growth stage. Since very few CIGS companies survive in such an intensively competitive photovoltaic market, it is difficult to conclude that the CIGS is in a growth stage. It is worth noting that new concept solar cells such as the perovskite solar cells are in an astonishing development in recent years, which might make the club of the thin film solar cells more uncertain. The prospect for the CIGS thin film solar cells is facing challenges coming from both the technology and market. For achieving the great expectation of the CIGS photovoltaics, there is still a long way to go.

## Acknowledgements

This work was supported by the Beijing Talent Cultivation Support Program for the Top Young Talents in Natural Science (2015000021223ZK38) and the National Natural Science Foundation of China under Grant No. 61404007.

## Author details

Yang Tang

Address all correspondence to: [tangy118@hotmail.com](mailto:tangy118@hotmail.com)

National Institute of Clean-And-Low-Carbon Energy, Future Science & Technology City,  
Beijing, People's Republic of China

## References

- [1] Green M A, Emery K, Hishikawa Y, Warta W, Dunlop ED. Solar cell efficiency tables (Version 39). *Progress in Photovoltaics: Research and Applications*, 2011; 20: 12–20. DOI: 10.1002/pip.2163
- [2] Press release, ZSW, June 15, 2016.
- [3] Sugimoto H. High efficiency and large volume production of CIS-based modules. 40th IEEE photovoltaic Specialists Conference, Denver, June 2014.
- [4] Press Release, First solar, February 23, 2016.
- [5] Press Release, First solar, July 15, 2015.
- [6] Sai H, Matsui T, Koida T, Matsubara K, Kondo M, Sugiyama S, Katayama H, Takeuchi Y, Yoshida I, Triple-junction thin-film silicon solar cell fabrication on periodically

- textured substrate with a stabilized efficiency of 13.6%. *Applied Physics Letters*, 2015; 106: 213902. DOI: 10.1063/1.4921794
- [7] Tel solar press release, July 9, 2014.
- [8] Komiya R, Fukui A, Murofushi N, Koide N, Yamanaka R, Katayama H, Improvement of the conversion efficiency of a monolithic type dye-sensitized solar cell module, Technical Digest, 21st International Photovoltaic Science and Engineering Conference, Fukuoka, November 2011, 2C-5O-08.
- [9] Hu H, Jiang K, Yang G, Li Z, Lin H, Liu Y, Zhao J, Zhang J, Huang F, Qu Q, Ma W, Yan H. Terthiophene-based D-A polymer with an asymmetric arrangement of alkyl chains that enables efficient polymer solar cells. *Journal of the American Chemical Society*, 2015; 137 (44), 14149–14157. DOI: 10.1021/jacs.5b08556
- [10] Hosoya M, Oooka H, Nakao H, Gotanda T, Mori S, Shida N, Hayase R, Nakano Y, Saito M. Organic thin film photovoltaic modules. Proceedings of the 93rd Annual Meeting of the Chemical Society of Japan, 2013; 21–37.
- [11] [http://www.nrel.gov/ncpv/images/efficiency\\_chart.jpg](http://www.nrel.gov/ncpv/images/efficiency_chart.jpg)
- [12] Chopra K L, Paulson P D, Dutta V, Thin-film solar cells: an overview. *Progress in Photovoltaics: Research and Applications*, 2004; 12: 69–92. DOI: 10.1002/pip.541
- [13] <https://commons.wikimedia.org/wiki/File:Chalcopyrite-unit-cell-3D-balls.png>
- [14] Bunn C W. *Proceedings of the Physical Society London*, 1935; 47: 835.
- [15] Heller R B, McGannon J, Weber A H. Precision determination of the lattice constants of zinc oxide. *Journal of Applied Physics*, 1950; 21: 1283. DOI: 10.1063/1.1699591
- [16] Gray T J. *Journal of the American Ceramic Society*, 1954; 37: 534.
- [17] Mohatny G P, Azaroff L V. Electron density distributions in ZnO crystals. *The Journal of Chemical Physics*, 1961; 35: 1268. DOI: 10.1063/1.1732035
- [18] Reeber R R. *Journal of Applied Physics*, 1970; 41: 506.
- [19] Özgür Ü, Alivov Y I, Liu C, Teke A, Reshchikov M A, Dogan S, Avrutin V, Cho S J, Morkoc H. A comprehensive review of ZnO materials and device. *Journal of Applied Physics*, 2005; 98: 041301. DOI: 10.1063/1.1992666.
- [20] [http://en.wikipedia.org/wiki/Solar\\_cell](http://en.wikipedia.org/wiki/Solar_cell)
- [21] Poormans J, Arkhipov V. *Thin Film Solar Cells Fabrication, Characterization and Applications*, John Wiley & Sons Ltd, England, 2006, p. xix.
- [22] Richards B S, Comparison of TiO<sub>2</sub> and other dielectric coatings for buried-contact solar cells: a review. *Progress in Photovoltaics*, 2004; 12: 253. DOI: 10.1002/pip.529
- [23] Aberle A G, Overview on SiN surface passivation of crystalline silicon solar cells. *Solar Energy Materials and Solar Cells*, 2001; 65: 239. DOI: 10.1016/S0927-0248(00)00099-4

- [24] Doshi P, Jellison G E, Rohatgi A. Characterization and optimization of absorbing plasma-enhanced chemical vapor deposited antireflection coatings for silicon photovoltaics. *Applied Optics*, 1997; 36: 7826. DOI: 10.1364/AO.36.007826
- [25] Ramanathan K, Contreras M A, Perkins C L, Asher S, Hasoon F S, Keane J, Young D, Romero M, Metzger W, Noufi R, Ward J, Duda A. *Progress in Photovoltaics* 2003; 11: 225. DOI: 10.1002/pip.494
- [26] Ae L, Kieven D, Chen J, Klenk R, Rissom Th, Tang Y, Lux-Steiner M Ch. *Progress in Photovoltaics: Research and Applications*, 2010; 18: 209-213. DOI: 10.1002/pip.946
- [27] Law M, Greene L E, Johnson J C, Saykally R, Yang P. Nanowire dye-sensitized solar cells. *Nature Materials*, 2005; 4: 455-45. DOI:10.1038/nmat1387
- [28] Sun X W, Chen J, Song J L, Zhao D W, Deng W Q, Lei W. Ligand capping effect for dye solar cells with a CdSe quantum dot sensitized ZnO nanorod photoanode. *Optics Express*, 2010; 18: 1296-1301. DOI: 10.1364/OE.18.001296
- [29] Olson D C, Shaheen S E, Collins R T, et al. The effect of atmosphere and ZnO morphology on the performance of hybrid poly(3-hexylthiophene)/ZnO nanofiber photovoltaic devices. *Journal of Physical Chemistry C*, 2007; 111: 16670-16678. DOI: 10.1021/jp0734225
- [30] Kim H W, Kim N H, Shim J H, Cho N H, Lee C. Catalyst-free MOCVD growth of ZnO nanorods and their structural characterization. *Journal of Materials Science: Materials in Electronics*, 2005; 16: 13.
- [31] Park W I, Yi G C, Jang H M. Metal-organic vapor phase epitaxial growth of high-quality ZnO films on Al<sub>2</sub>O<sub>3</sub>(001). *Journal of Materials Research*, 2001; 16: 1358. DOI: 10.1557/JMR.2001.0190
- [32] Huang M H, Wu Y, Feick H, Tran N, Weber E, Yang P. Catalytic growth of zinc oxide nanowires by vapor transport. *Advanced Materials*, 2001; 13: 113. DOI: 10.1002/1521-4095(200101)13:2<113::AID-ADMA113>3.0.CO;2-H
- [33] Umar A, Kim S H, Suh E-K, Hahn Y B. *Nanotechnology*, 2006, 17, 4072.
- [34] He J H, Wang C W, Liao K F, Chen L J. *Advances in Science and Technology*, 2006, 51, 38.
- [35] Izaki M, Omi T. Transparent zinc oxide films prepared by electrochemical reaction. *Applied Physics Letters*, 1996; 68: 2439-2440. DOI: 10.1063/1.116160
- [36] Izaki M, Omi T, Structural and optical properties of single-crystalline ZnO nanorods grown on silicon by thermal evaporation. *Journal of The Electrochemical Society*, 1996; 143: L53-55. DOI: 10.1088/0957-4484/17/16/013
- [37] Lan C J, Cheng H Y, Chung R J, Li J H, Kao K F, Chin T S, Bi-doped ZnO layer prepared by electrochemical deposition. *Journal of The Electrochemical Society*, 2007; 154: D117-D12. DOI: 10.1149/1.2422887

- [38] Yang J, Qiu Y, Yang S. Studies of electrochemical synthesis of ultrathin ZnO nanorod/nanobelt arrays on Zn substrates in alkaline solutions of amine-alcohol mixtures. *Crystal Growth & Design*, 2007; 7: 2562-2567. DOI: 10.1021/cg070513i
- [39] Chen J, Ae L, Aichele Ch, Lux-Steiner M Ch. High internal quantum efficiency ZnO nanorods prepared at low temperature. *Applied Physics Letters*, 2008, 92, 161906. DOI: 10.1063/1.2910769
- [40] Vayssieres L, Keis K, Lindquist S E. Purpose-built anisotropic metal oxide material: 3D highly oriented microrod array of ZnO. *The Journal of Physical Chemistry B*, 2001; 105: 3350. DOI: 10.1021/jp010026s
- [41] Schmidt-Mende L, MacManus-Driscoll J L. ZnO – nanostructures, defects, and devices. *Materials Today*, 2007; 10: 40. DOI: 10.1016/S1369-7021(07)70078-0
- [42] Ashfold M N R, Doherty R P, Ndifor-Angwafor N G, Riley D J, Sun Y. The kinetics of the hydrothermal growth of ZnO nanostructures. *Thin Solid Films*, 2007; 515: 8679. DOI: 10.1016/j.tsf.2007.03.122
- [43] Govender K, Boyle D S, Kenway P B, O'Brien P. Understanding the factors that govern the deposition and morphology of thin films of ZnO from aqueous solution. *Journal of Materials Chemistry*, 2004; 14: 2575. DOI: 10.1039/B404784B
- [44] Greene L E, Law M, Goldberger J. Low-temperature wafer-scale production of ZnO nanowire arrays. *Angewandte Chemie International Edition*, 2003, 42, 3031-3034. DOI: 10.1002/anie.200351461
- [45] Tak Y, Yong K. Controlled growth of well-aligned ZnO nanorod array using a novel solution method. *The Journal of Physical Chemistry B*, 2005; 109: 19263-19269. DOI: 10.1021/jp0538767
- [46] Lin C-C, Chen H-P, Liao H-C, Chen S-Y. Enhanced luminescent and electrical properties of hydrogen-plasma ZnO nanorods grown on wafer-scale flexible substrates. *Applied Physics Letters*, 2005, 86, 183103. DOI: 10.1063/1.1904715
- [47] Bagotsky V S. *Fundamentals of Electrochemistry*, John Wiley & Sons, Inc., New Jersey, 2006, second edition, p. 10.
- [48] Bagotsky V S. *Fundamentals of Electrochemistry*, John Wiley & Sons, Inc., New Jersey, 2006, second edition, p. 191.
- [49] Shiosaki T, Ohnishi S, Hirokawa Y, Kawabata A. *Applied Physics Letters*, 1978, 33, 406. DOI: 10.1063/1.90393